ARTICLE　　OPEN

Check for updates

Glucocorticoid stress hormones stimulate vesicle-free Tau secretion and spreading in the brain

Qing Yu[1,6], Fang Du[1,6], Irla Belli[1], Patricia A. Gomes [2,3], Ioannis Sotiropoulos[2,3,4] and Clarissa L. Waites [1,5✉]

Chronic stress and elevated levels of glucocorticoids (GCs), the main stress hormones, accelerate Alzheimer's disease (AD) onset and progression. A major driver of AD progression is the spreading of pathogenic Tau protein between brain regions, precipitated by neuronal Tau secretion. While stress and high GC levels are known to induce intraneuronal Tau pathology (*i.e.* hyperphosphorylation, oligomerization) in animal models, their role in trans-neuronal Tau spreading is unexplored. Here, we find that GCs promote secretion of full-length, primarily vesicle-free, phosphorylated Tau from murine hippocampal neurons and ex vivo brain slices. This process requires neuronal activity and the kinase GSK3β. GCs also dramatically enhance trans-neuronal Tau spreading in vivo, and this effect is blocked by an inhibitor of Tau oligomerization and type 1 unconventional protein secretion. These findings uncover a potential mechanism by which stress/GCs stimulate Tau propagation in AD.

INTRODUCTION

Stressful life events and high circulating levels of glucocorticoids (GCs), the primary stress hormones, are known risk factors for Alzheimer's disease (AD) [1–3]. Indeed, epidemiological and clinical studies suggest that prolonged psychosocial stress significantly elevates AD risk, and high GC levels are associated with faster cognitive decline in AD patients [1–5]. Moreover, stress interacts with genetic risk factors to hasten the onset of AD symptoms and pathology in both animal models and humans [6–12]. Stress and AD appear to share a common pathological driver: the microtubule-associated protein Tau. Not only do stress and high GC levels trigger Tau pathology similar to that seen in AD brain tissue (i.e., Tau hyperphosphorylation and aggregation) [13–15], but Tau depletion is protective against both amyloid beta- and stress-induced neurotoxicity and cognitive impairment in animal models [15–17], indicating Tau's essential role as a mediator of neurodegeneration in the context of AD and chronic stress.

A key feature of Tau pathology in AD is its stereotypical spreading pattern between anatomically connected brain regions (entorhinal cortex to hippocampus to prefrontal cortex) [18]. This spreading is highly correlated with the severity of cognitive impairment in AD patients and appears to be a major driver of AD progression [18–20]. Given the relationship between Tau propagation and clinical AD symptoms, there has been tremendous interest in elucidating the mechanisms of Tau secretion and spreading in the brain. Numerous studies have shown that Tau is secreted from neurons in extracellular vesicles, including ectosomes that derive from the plasma membrane and exosomes that derive from multivesicular endosomes of the endolysosomal pathway, and also as vesicle-free protein [21–23].

While vesicle-mediated mechanisms of Tau spreading have been a focus of study for over a decade [21, 24, 25], the vast majority of Tau secreted by neurons (~90%) is vesicle-free [23, 25–32], and considerably less is known about this mode of secretion and its contribution to pathogenic Tau propagation. Similarly, although chronic stress and high GC levels are known to induce Tau pathology in the hippocampus and cortex, precipitating synaptic loss and behavioral impairment in animal models (i.e. anxiety, anhedonia, learning/memory deficits) [14, 15, 33], it is unclear whether or how stress/GCs stimulate the spreading of Tau pathology between these brain regions.

In the current study, we investigate the effects of GCs on neuronal Tau secretion and spreading in murine hippocampal neurons, brain slices, and in vivo hippocampus. We find that GCs induce secretion of predominantly vesicle-free Tau in an activity- and glycogen synthase kinase 3β (GSK3β)-dependent manner, and provide evidence that this process occurs through type 1 unconventional protein secretion (UPS). Moreover, we show that GC administration stimulates Tau spreading through the hippocampus, and that this effect is prevented by inhibiting Tau aggregation and type 1 UPS with the catechin epigallocatechin gallate (EGCG). Together, these findings demonstrate that elevated GC levels promote Tau propagation, and suggest a mechanism by which stress/GCs speed cognitive decline in AD.

RESULTS

To determine whether GCs stimulate neuronal Tau secretion, we measured extracellular Tau levels by immunoblot and/or ELISA in

[1]Department of Pathology and Cell Biology, Taub Institute for Research on Alzheimer's Disease and Aging Brain, Columbia University Irving Medical Center, New York, NY, USA. [2]Life and Health Sciences Research Institute (ICVS), School of Medicine, University of Minho, Campus de Gualtar, Braga, Portugal. [3]ICVS/3B's - PT Government Associate Laboratory, Braga/Guimarães, Portugal. [4]Institute of Biosciences and Applications, National Centre for Scientific Research (NCSR) Demokritos, Agia Paraskevi, Greece. [5]Department of Neuroscience, Columbia University, New York, NY, USA. [6]These authors contributed equally: Qing Yu, Fang Du. ✉email: cw2622@cumc.columbia.edu
Edited by Professor Giampietro Schiavo
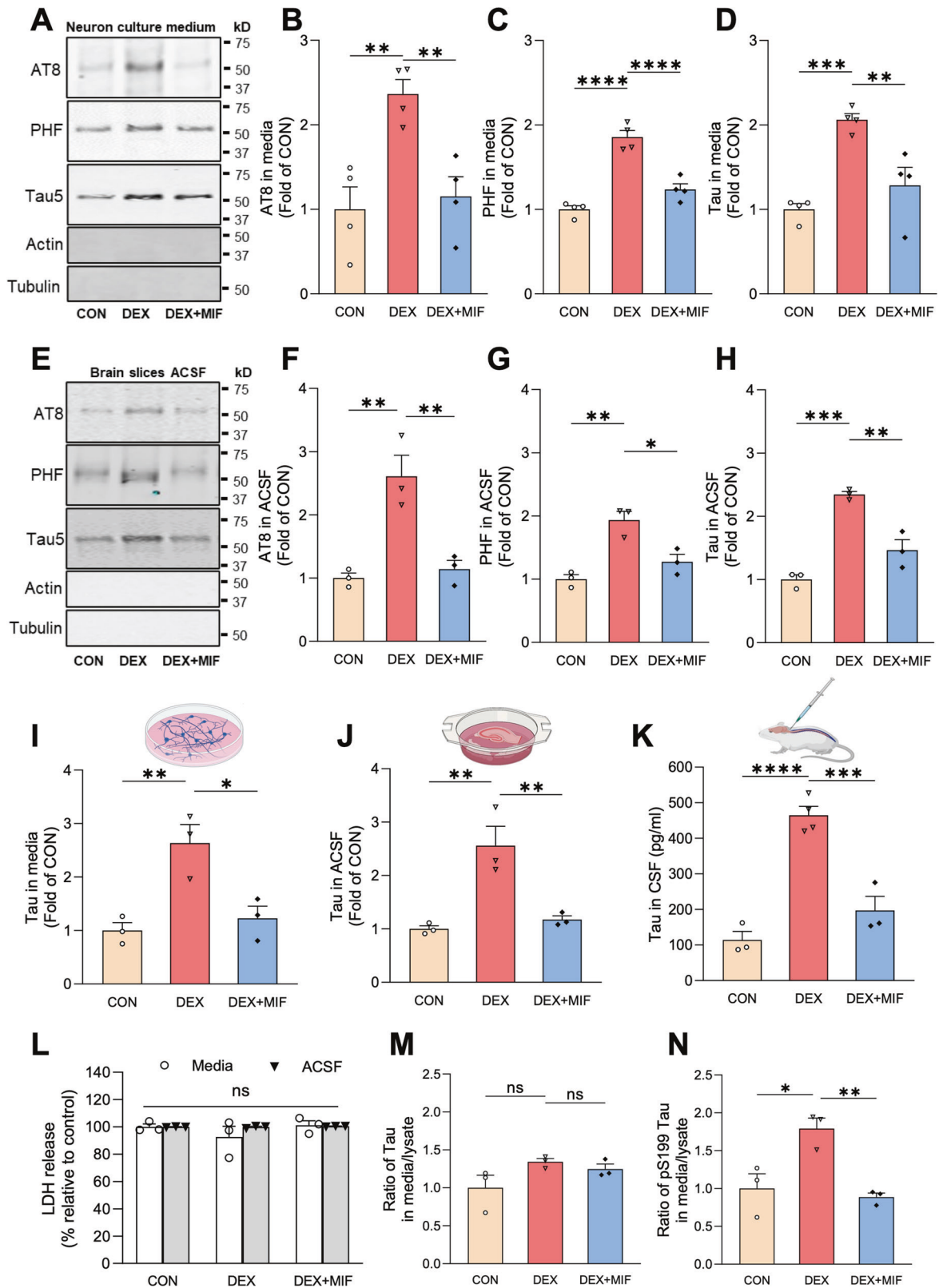
three preparations: (1) media from 14 day in vitro (DIV) wild-type murine hippocampal neurons treated for 48 h with vehicle control, the synthetic GC dexamethasone (DEX), or DEX + GC receptor (GR) antagonist mifepristone (MIF) (Fig. 1A–D, I), (2) artificial cerebrospinal fluid (ACSF) from ex vivo brain slices of 4-month old wild-type mice, perfused for 4 h with vehicle, DEX, or DEX + MIF (Fig. 1E–H, J), and (3) CSF from 4-5-month old wild-type mice administered vehicle, DEX, or DEX + MIF for 15 days (Fig. 1K). The efficacy of DEX treatment was confirmed by immunoblotting hippocampal lysates for phospho-GR and by immunostaining for

Fig. 1 Glucocorticoids induce secretion of vesicle-free, phosphorylated Tau. A–D Representative immunoblots **A** and quantification **B–D** of AT8, PHF1, and total Tau (Tau5) immunoreactivity in extracellular vesicle (EV)-depleted media from hippocampal neurons treated with vehicle (CON), DEX, or DEX + MIF. Intensity values are normalized to the CON condition (**$P_{CON\ VS.\ DEX}$ = 0.0054, **$P_{DEX\ VS.\ DEX\ +\ MIF}$ = 0.0109 for **B**, ****$P_{CON\ VS.\ DEX}$ < 0.0001, ****$P_{DEX\ VS.\ DEX\ +\ MIF}$ = 0.0002 for **C**, ***$P_{CON\ VS.\ DEX}$ = 0.0010, **$P_{DEX\ VS.\ DEX\ +\ MIF}$ = 0.0074 for **D**, one-way ANOVA with Tukey's multiple comparisons test). **E–H** Representative immunoblots **E** and quantification **F–H** of AT8, PHF1, and total Tau (Tau5) immunoreactivity in EV-depleted ACSF from brain slices perfused with vehicle (CON), DEX, or DEX + MIF. Intensity values are normalized to the CON condition (**$P_{CON\ VS.\ DEX}$ = 0.0042, **$P_{DEX\ VS.\ DEX\ +\ MIF}$ = 0.0066 for **F**, **$P_{CON\ VS.\ DEX}$ = 0.0026, *$P_{DEX\ VS.\ DEX\ +\ MIF}$ = 0.0144 for **G**, ***$P_{CON\ VS.\ DEX}$ = 0.0003, **$P_{DEX\ VS.\ DEX\ +\ MIF}$ = 0.0029 for **H**, one-way ANOVA with Tukey's multiple comparisons test). **I–K** Quantification of ELISA for total Tau levels in EV-depleted media from hippocampal neurons (**I**), ACSF from brain slices **J**, and CSF from mice **K** following the indicated treatments. Values are normalized to CON condition in **I**, **J** and expressed as pg/ml in **K** (**$P_{CON\ VS.\ DEX}$ = 0.0093, *$P_{DEX\ VS.\ DEX\ +\ MIF}$ = 0.0185 for **I**, **$P_{CON\ VS.\ DEX}$ = 0.0055, **$P_{DEX\ VS.\ DEX\ +\ MIF}$ = 0.0097 for **J**, ***$P_{CON\ VS.\ DEX}$ = 0.0002, ***$P_{DEX\ VS.\ DEX\ +\ MIF}$ = 0.0008 for **K**, one-way ANOVA with Tukey's multiple comparisons test). **L** Quantification of LDH in extracellular vesicle (EV)-depleted media (white bars) or ACSF (gray bars) from the indicated treatment conditions ($P_{CON\ VS.\ DEX}$ = 0.3465, $P_{DEX\ VS.\ DEX\ +\ MIF}$ = 0.2517 for media samples, $P_{CON\ VS.\ DEX}$ > 0.9999, $P_{DEX\ VS.\ DEX\ +\ MIF}$ = 0.9941 for ACSF samples, two-way ANOVA with Tukey's multiple comparisons test). **M, N** Ratio of Tau concentration in neuronal media to Tau concentration in neuronal lysate for CON and DEX conditions, measured by ELISA, for total Tau **M** and pS199 Tau **N** ($P_{CON\ VS.\ DEX}$ = 0.1339, $P_{DEX\ VS.\ DEX\ +\ MIF}$ = 0.8068 for **M**, *$P_{CON\ VS.\ DEX}$ = 0.0182, **$P_{DEX\ VS.\ DEX\ +\ MIF}$ = 0.0098 for **N**, one-way ANOVA with Tukey's multiple comparisons test). Data is presented as mean ± SEM with n = 3–4 samples/group (results were confirmed in two independent experiments).

phospho- and oligomeric Tau (Fig. S1A–E), as in our recent study [34]. In all three preparations, DEX significantly increased Tau concentration compared to vehicle and DEX + MIF (Fig. 1A–K). This increase in extracellular Tau did not result from cell death or disruption of plasma membrane integrity, as lactate dehydrogenase (LDH) levels were unaltered by DEX ± MIF in both the in vitro and ex vivo preparations (Fig. 1L), and the abundant cytoskeletal proteins actin and tubulin were not detected in these fluids (Fig. 1A, E). Moreover, extracellular Tau was ~55 kD (around the reported size for full-length Tau protein) and phosphorylated at multiple sites, as demonstrated by immunoreactivity against common phospho-Tau epitopes detected by the AT8 (pSer202/pThr205) and PHF1 (pSer396/pSer404) antibodies (Fig. 1A, E). Media from DEX-treated neurons also exhibited immunoreactivity against the TOMA-1 antibody [35], indicating the presence of oligomeric Tau (Fig. S1F). However, in contrast to Tau in neuronal lysates following 48-hour DEX administration (Fig. S1G–K), secreted Tau was not enriched in AT8 and PHF1 phospho-Tau epitopes when normalized to total Tau levels (Fig. S1L–O), indicating no specific enrichment of Tau phosphorylated at these sites. Secreted Tau also appeared to be primarily vesicle-free rather than associated with extracellular vesicles (EVs), which were almost completely depleted from media and ACSF by a well-established centrifugation procedure (Fig. S1P–R) [36, 37]. Extracellular Tau levels were similarly increased in media containing cortical and hippocampal brain slices from mice subjected chronic unpredictable stress (CUS) compared to control conditions (Fig. S1S–V), demonstrating that CUS and GC exposure have comparable stimulatory effects on Tau secretion.

Since stress/GCs promote Tau accumulation, these findings could reflect similar levels of Tau secretion from a larger intraneuronal pool. To determine whether GCs alter the fractional amount of Tau secreted from neurons, we measured Tau concentration in media versus neuronal lysate for control and DEX conditions, using ELISA kits to detect total or pS199 phospho-Tau. Interestingly, DEX treatment did not change the secreted versus intracellular ratio for total Tau (Fig. 1M), but significantly increased this ratio for pS199 Tau (by two-fold; Fig. 1N). These results indicate that DEX preferentially stimulates secretion of S199 phospho-Tau.

Secretion of vesicle-free Tau has been shown to occur through type 1 UPS, wherein Tau is directly translocated across the plasma membrane through interactions with heparin sulfate proteoglycans (HSPGs), cholesterol, and sphingolipids [38, 39]. To determine whether GCs stimulate Tau secretion via this pathway, we first treated hippocampal neurons and brain slices from wild-type mice with vehicle or DEX +/- NaClO₃, an inhibitor of HSPG synthesis previously shown to decrease Tau secretion via type 1 UPS [38, 39]. Following media/ACSF collection, EV depletion, and

measurement of total and phospho-Tau levels by immunoblot and ELISA, we found that $NaClO_3$ almost completely blocked the DEX-induced increase in extracellular Tau levels (Fig. 2A–H, S2A, B). Treatment with methyl-β-cyclodextrin to extract membrane cholesterol similarly inhibited DEX-induced Tau secretion in neuronal cultures and brain slices (Fig. 2I–P, Fig. S2C, D), demonstrating its HSPG- and cholesterol-dependence. As in previous experiments, these treatments did not alter the ratio of AT8 or PHF1 to total Tau (Fig. S2E–L), indicating no change in pSer202/pThr205 or pSer396/pSer404 phospho-Tau epitopes. Since type 1 UPS is ATP-independent, we also tried to confirm this aspect of DEX-induced Tau secretion. Unfortunately, the different time courses of DEX treatment vs. ATP depletion with 2-deoxyglucose, and the toxicity of this latter treatment, prevented us from testing both conditions simultaneously. However, we did verify that baseline Tau secretion in our neuronal cultures was ATP-independent, by briefly incubating neurons with 2-deoxyglucose (30 mM, 1 hr). Here, we used hippocampal neurons cultured from transgenic PS19 mice (overexpressing human P301S mutant Tau), which secrete higher levels of Tau at baseline and therefore enable detection of extracellular Tau within the 1-hour timeframe. While 2-deoxyglucose reduced cellular ATP production by ~70%, it did not change the concentration of extracellular Tau in EV-depleted medium (Fig. S2M), confirming the overall ATP-independence of Tau secretion measured in our assays.

GCs are known to induce Tau hyperphosphorylation via activation of Tau kinases (e.g. GSK3β, CDK5) [13, 40–42] and also to stimulate neuronal firing [43–45], both of which are reported to enhance Tau secretion [26, 38, 39]. We therefore treated hippocampal neurons with DEX±the GSK3β inhibitor TDZD-8 or the Na⁺ channel blocker tetrodotoxin (TTX) to inhibit neuronal firing. Both treatments prevented the DEX-induced increase in Tau phosphorylation as measured by the PHF1/total Tau ratio in immunoblots from neuronal lysates (Fig. S2N, O). Similarly, both treatments blocked DEX-induced Tau secretion as measured by immunoblots and ELISA for total and phospho-Tau (Fig. 3A–E, H–L). However, neither drug significantly altered AT8/total Tau or PHF1/total Tau ratios in the secreted Tau pool (Fig. 3F, G, M, N), suggesting that pSer202/pThr205 and pSer396/pSer404 epitopes are not the primary drivers of Tau secretion. Nevertheless, these findings indicate that GC-induced Tau secretion is dependent upon neuronal activity and GSK3β-mediated Tau phosphorylation.

Trans-cellular spreading of pathogenic Tau is regarded as a key driver of AD progression [22]. We therefore examined whether Tau secreted in response to high GC levels is internalized by neighboring neurons. For these experiments, we harvested media from PS19 'donor' hippocampal neurons (expressing hTau) and added it to 'recipient' neurons from wild-type mice (Fig. 4A),
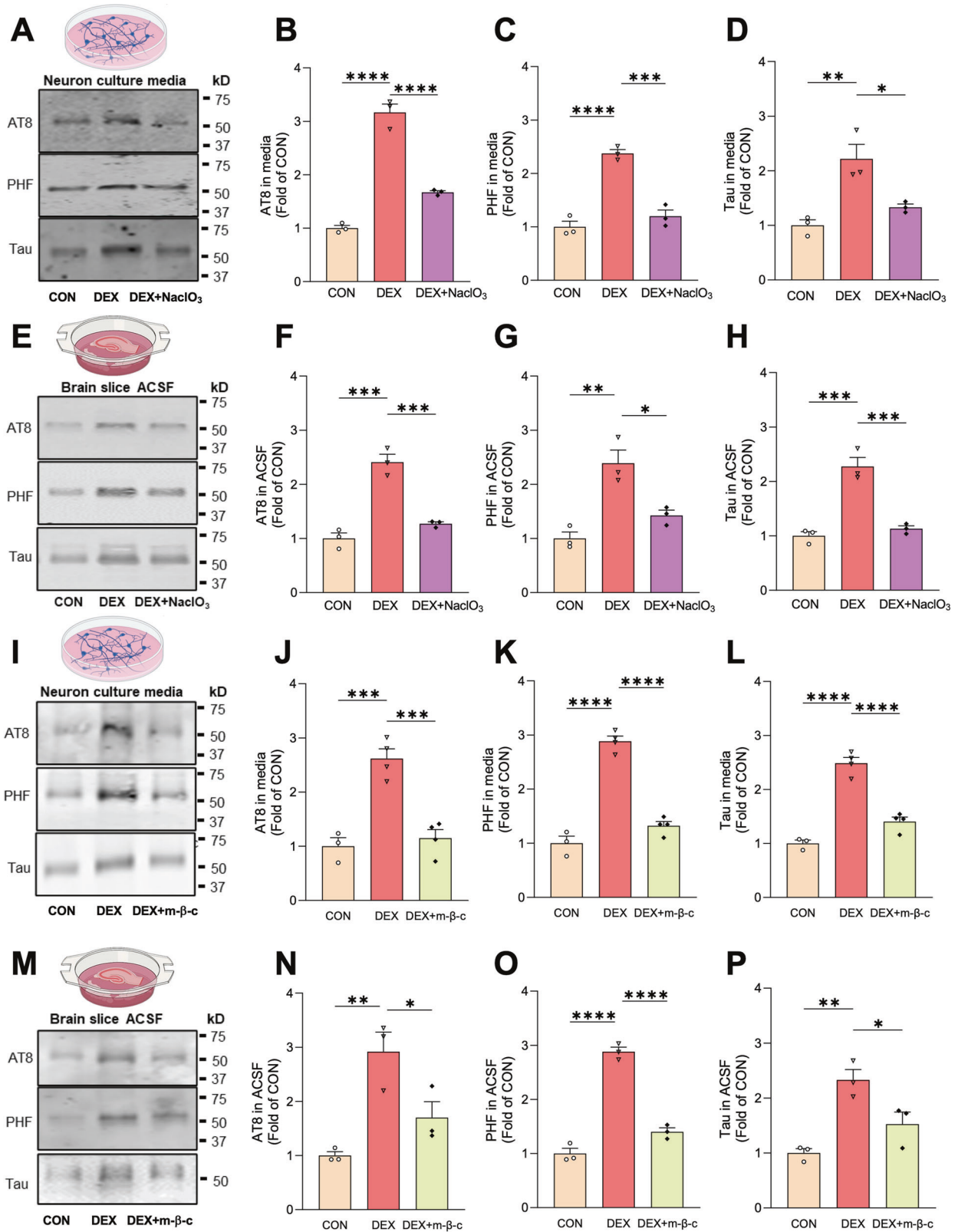
enabling us to quantify Tau uptake by immunostaining with human-specific anti-Tau13 antibodies. After verifying by ELISA that PS19 neurons also undergo DEX-dependent Tau secretion (Fig. 4B), we harvested media from these neurons (following 48-h treatment with either vehicle or 1 µM DEX) and added it to recipient neurons for 48 h (Fig. 4A, C). Quantification of Tau uptake revealed that hTau secreted by both control and DEX-treated PS19 donor neurons was readily taken up by recipient neurons (Fig. 4C, D), indicative of its ability to spread trans-cellularly. This result was anticipated based on previous studies [38, 39].

Fig. 2 GC-mediated Tau secretion is blocked by inhibitors of type 1 unconventional protein secretion. A–C Representative immunoblots **A** and quantification **B–D** of AT8, PHF1, and total Tau immunoreactivity in EV-depleted media from hippocampal neurons treated with vehicle (CON), DEX, or DEX + $NaClO_3$. Intensity values are normalized to CON condition (****$P_{CON \, VS. \, DEX}$ < 0.0001, ****$P_{DEX \, VS. \, DEX \, + \, NaClO3}$ < 0.0001 for **B**, ***$P_{CON \, VS. \, DEX}$ = 0.0002, ***$P_{DEX \, VS. \, DEX \, + \, NaClO3}$ = 0.0004 for **C**, **$P_{CON \, VS. \, DEX}$ = 0.0051, *$P_{DEX \, VS. \, DEX \, + \, NaClO3}$ = 0.0223 for for **D**; one-way ANOVA with Tukey's multiple comparisons test). **E–H** Representative immunoblots **E** and quantification **F–H** of AT8, PHF1, and total Tau immunoreactivity in EV-depleted ACSF from brain slices perfused with vehicle (CON), DEX, or DEX + $NaClO_3$. Intensity values are normalized to CON condition (***$P_{CON \, VS. \, DEX}$ = 0.0002, ***$P_{DEX \, VS. \, DEX \, + \, NaClO3}$ = 0.0006 for **F**, **$P_{CON \, VS. \, DEX}$ = 0.0026, *$P_{DEX \, VS. \, DEX \, + \, NaClO3}$ = 0.0151 for **G**, ***$P_{CON \, VS. \, DEX}$ = 0.0004, ***$P_{DEX \, VS. \, DEX \, + \, NaClO3}$ = 0.0008 for **H**; one-way ANOVA with Tukey's multiple comparisons test). **I–L** Representative immunoblots **I** and quantification **J–L** of AT8, PHF1, and total Tau immunoreactivity in EV-depleted media from hippocampal neurons treated with vehicle (CON), DEX, or DEX + methyl-β-cyclodextrin (m-β-c). Intensity values are normalized to CON condition (***$P_{CON \, VS. \, DEX}$ = 0.0005, ***$P_{DEX \, VS. \, DEX \, + \, m-β-c}$ = 0.0005 for **J**, ****$P_{CON \, VS. \, DEX}$ < 0.0001, ****$P_{DEX \, VS. \, DEX \, + \, m-β-c}$ < 0.0001 for **K**, ****$P_{CON \, VS. \, DEX}$ < 0.0001, ****$P_{DEX \, VS. \, DEX \, + \, m-β-c}$ < 0.0001 for **L**; one-way ANOVA with Tukey's multiple comparisons test). **M–P** Representative immunoblots **M** and quantification **N–P** of AT8, PHF1, and total Tau immunoreactivity in ACSF from brain slices perfused with vehicle (CON), DEX, or DEX + methyl-b-cyclodextrin (m-β-c). Intensity values are normalized to CON condition (**$P_{CON \, VS. \, DEX}$ = 0.0060, *$P_{DEX \, VS. \, DEX \, + \, m-β-c}$ = 0.0447 for **N**, ****$P_{CON \, VS. \, DEX}$ < 0.0001, ****$P_{DEX \, VS. \, DEX \, + \, m-β-c}$ < 0.0001 for **O**, **$P_{CON \, VS. \, DEX}$ = 0.0040, *$P_{DEX \, VS. \, DEX \, + \, m-β-c}$ = 0.0396 for **P**; one-way ANOVA with Tukey's multiple comparisons test). Data is presented as mean ± SEM with n = 3–4 samples/group (results were confirmed in two independent experiments).

However, hTau levels were three-fold higher in recipient neurons incubated with medium from DEX-treated donor cells versus vehicle-treated cells (Fig. 4D). This finding likely reflects increased hTau levels in media following DEX treatment in donor cells, but could also indicate a stimulatory effect of DEX on Tau uptake by recipient cells, or DEX-related toxicity leading to increased membrane permeability to Tau. To investigate these latter possibilities, we treated recipient neurons with DEX for 48 h during their incubation with (control) donor cell medium and subsequently quantified hTau levels. Interestingly, DEX-treated recipient neurons exhibited similar levels of hTau as their vehicle-treated counterparts (Fig. 4C, D), and no difference in LDH release (Fig. 4E). These findings indicate that GCs do not stimulate Tau internalization or alter plasma membrane permeability, but rather facilitate Tau spreading by stimulating its secretion.

Finally, we evaluated whether high circulating GC levels promote Tau spreading in vivo. Here, 4-5-month-old wild-type male mice (3/ group) were pre-treated with vehicle, DEX, or DEX + MIF for 7 days, then injected in hippocampal area CA1 (Fig. 5A) with an adeno-associated virus (AAV) that enables visualization of trans-cellular Tau spreading (AAV.CBA.eGFP.2 A.P301L-Tau) [46]. Animals were then treated for an additional 14 days with vehicle (CON), DEX, or DEX + MIF prior to tissue harvest. DEX administration caused a ~ 10% loss of body weight during this time period, demonstrating its ability to promote an endocrine response (Fig. S2P). After brains from each treatment group were harvested and sectioned, human P301LTau spreading was evaluated by immunostaining with anti-Tau13 antibodies (Fig. 5B, C). Tau propagation was quantified as in previous studies [46, 47], by counting hTau$^+$/GFP$^-$ neurons per mm^2 near the injection site and calculating the ratio of hTau$^+$ cells expressing GFP (GFP/hTau colocalization) (Fig. 5D, E). Remarkably, the number of hTau$^+$/GFP$^-$ neurons was dramatically increased in DEX-treated animals compared to CON or DEX + MIF conditions (Fig. 5B, D), while GFP/hTau colocalization was significantly decreased (Fig. 5B, E). AAV transduction efficiency (number of GFP$^+$ cells per mm^2) was similar across treatment conditions (Fig. 5F). Moreover, in DEX-treated animals, hTau was detected in brain areas more than 1000 µm away from GFP$^+$ neurons, a phenomenon not observed in the other groups (Fig. 5C, G; Fig. S3A–D). These data demonstrate that GCs strongly promote Tau secretion and spreading in vivo. To assess whether this spreading is likely to occur via type 1 UPS, we initiated a second hTau spreading experiment with epigallocatechin gallate (EGCG), a potent inhibitor of Tau aggregation that attenuates its secretion via type 1 UPS [38, 48] and can be used in vivo, unlike other inhibitors of this secretory mechanism [49, 50]. We first verified the ability of EGCG to reduce GC-induced Tau secretion in brain slices (Fig. S3E–I). Animals were then subjected to the same experimental paradigm as above, but with EGCG instead of MIF. We again found that DEX provoked a ~10% loss of body weight, and

this phenotype was not rescued by EGCG (similar to MIF treatment; Fig. S2P). As predicted by its ex vivo efficacy, EGCG administration almost completely prevented DEX-induced Tau spreading in the hippocampus (Fig. 5H–M; Fig. S3D), showing that this process occurs via Tau oligomerization and secretion, likely via type 1 UPS.

DISCUSSION

This work provides the first demonstration that GCs stimulate Tau spreading in the brain, implicating these stress hormones in both the initial stages of Tau pathogenesis, by inducing Tau hyperphosphorylation and aggregation within neurons, and subsequently in the transmission of pathogenic Tau between neurons. We show that GCs likely stimulate Tau secretion via type 1 UPS, an ATP-independent process requiring interactions between phosphorylated/oligomeric Tau and plasma membrane-associated HSPGs and lipids. Notably, Tau secretion and spreading have also been shown to occur via extracellular vesicles (i.e. exosomes and ectosomes) and to be mediated by other brain cell types including microglia [24, 51]. Additional work will be required to determine whether GCs also stimulate Tau propagation via these mechanisms.

An intriguing finding of this study is that EGCG, a catechin found at high levels in green tea leaves, blocks GC-induced Tau spreading in vivo. EGCG is an inhibitor of Tau oligomerization and aggregation as well as its secretion via type 1 UPS, suggesting that this is an important mode of GC-driven Tau propagation. However, EGCG also alters lipid membrane properties [52, 53] and could alter Tau secretion/uptake via this mechanism. Other drugs that block type 1 UPS, such as $NaClO_3$ and methyl-β-cyclodextrin, have similarly pleiotropic effects (and further cannot be used in vivo due to their blood brain barrier impermeability and toxicity, respectively [49, 50]), making it difficult to definitively demonstrate that secretion via type 1 UPS is the primary driver of GC-induced Tau propagation in vivo. However, given the relative amount of Tau reported to undergo secretion in vesicle-free form (~90%) [22], together with our in vitro and ex vivo findings showing that $NaClO_3$ and methyl-β-cyclodextrin strongly attenuate DEX-mediated Tau secretion, we think it likely that type 1 UPS contributes substantially to GC-induced Tau spreading in vivo.

Our experiments further reveal that GCs promote Tau secretion by stimulating GSK3β-mediated Tau phosphorylation. GSK3β, a brain-enriched serine/threonine kinase implicated in Tau pathogenesis in AD, phosphorylates multiple Tau residues, including those detected by our ELISA (S199) and immunoblotting (Ser202/Thr205, S396/S404) assays [54, 55]. Indeed, we observe that GCs selectively increase secretion of pS199 Tau compared to total Tau, and the GSK3β inhibitor TDZD-8 effectively blocks GC-mediated Tau secretion in hippocampal neurons. At the same time, GCs do
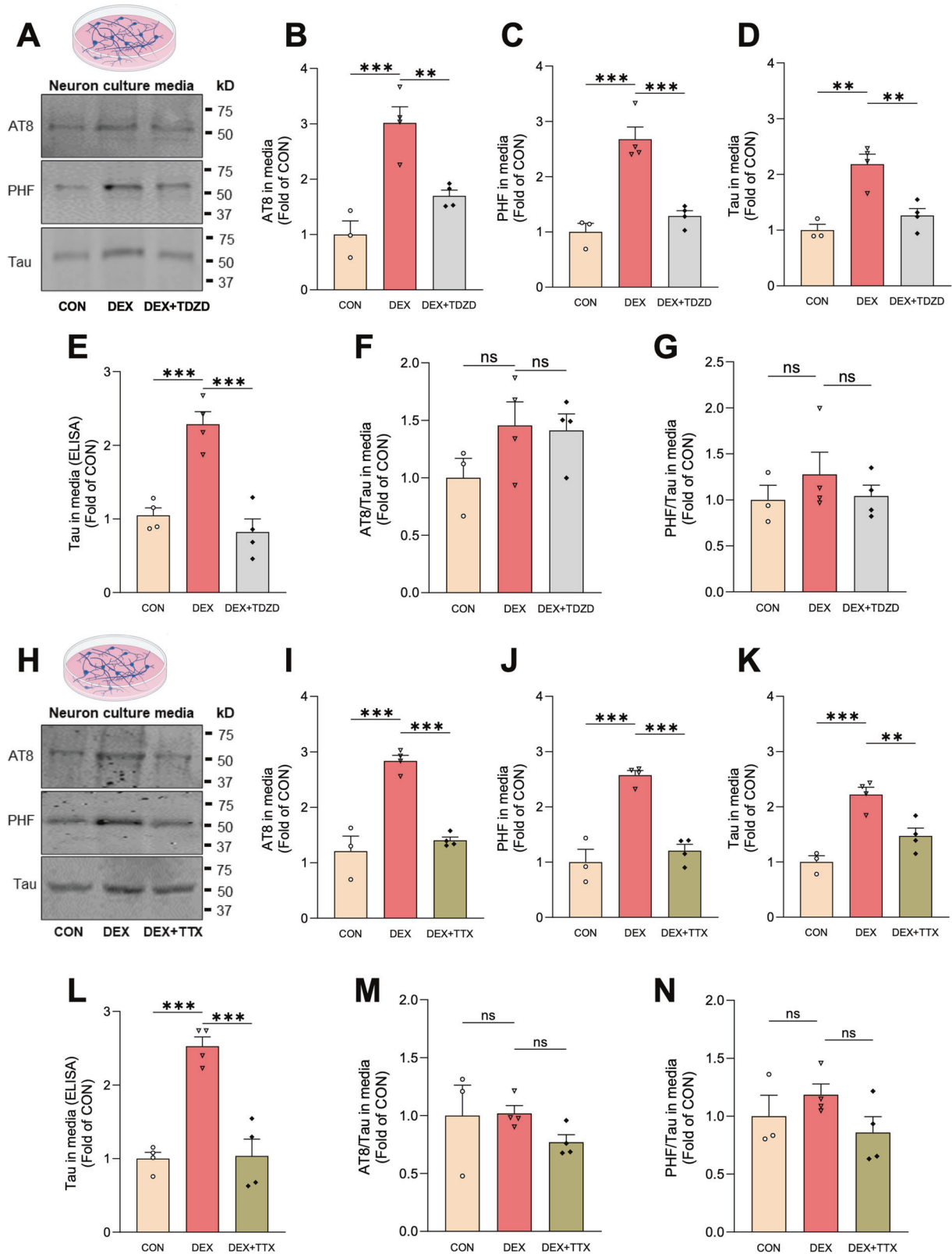
not promote the enrichment of secreted Tau phosphorylated at Ser202/Thr205 or S396/S404 as detected by AT8 and PHF1 antibodies, indicating that these common phospho-sites are not the drivers of Tau secretion. Indeed, previous work indicates that overall phosphorylation state rather than the phosphorylation of specific residues drives Tau secretion via type 1 UPS [39], in agreement with our findings.

Interestingly, we also find that neuronal activity is critical for GC-induced Tau phosphorylation and secretion, as treatment with TTX to inhibit action potential firing prevents both events. These data

Fig. 3 GC-induced Tau secretion is attenuated by inhibitors of GSK3β and neuronal activity. A–D Representative immunoblots **A** and quantification **B–D** of AT8, PHF1, and total Tau immunoreactivity in media from hippocampal neurons treated with vehicle (CON), DEX, or DEX + TDZD-8. Intensity values are normalized to CON condition (***$P_{CON\ VS.\ DEX}$ = 0.0007, **$P_{DEX\ VS.\ DEX\ +\ TDZD}$ = 0.0064 for **B**, ***$P_{CON\ VS.\ DEX}$ = 0.0003, ***$P_{DEX\ VS.\ DEX\ +\ TDZD}$ = 0.0007 for **C**, **$P_{CON\ VS.\ DEX}$ = 0.0016, **$P_{DEX\ VS.\ DEX\ +\ TDZD}$ = 0.0045 for **D**; one-way ANOVA with Tukey's multiple comparisons test). **E** Quantification of ELISA for total Tau levels in EV-depleted media from the indicated conditions, with values normalized to CON condition (***$P_{CON\ VS.\ DEX}$ = 0.0008, ***$P_{DEX\ VS.\ DEX\ +\ TDZD}$ = 0.0002, one-way ANOVA with Tukey's multiple comparisons test). **F, G** Quantification of AT8/total Tau **F** and PHF1/total Tau **G** ratios, showing no significant difference between the indicated conditions ($P_{CON\ VS.\ DEX}$ = 0.2437, $P_{DEX\ VS.\ DEX\ +\ TDZD}$ = 0.9825 for **F**, $P_{CON\ VS.\ DEX}$ = 0.5867, $P_{DEX\ VS.\ DEX\ +\ TDZD}$ = 0.6339 for **G**, one-way ANOVA with Tukey's multiple comparisons test). **H–K** Representative immunoblots **H** and quantification **I–K** of AT8, PHF1, and total Tau immunoreactivity in media from hippocampal neurons treated with vehicle (CON), DEX, or DEX + TTX. Intensity values are normalized to CON condition (***$P_{CON\ VS.\ DEX}$ = 0.0001, ***$P_{DEX\ VS.\ DEX\ +\ TTX}$ = 0.0002 for **I**, ***$P_{CON\ VS.\ DEX}$ = 0.0001, ***$P_{DEX\ VS.\ DEX\ +\ TTX}$ = 0.0002 for **J**, ***$P_{CON\ VS.\ DEX}$ = 0.0007, **$P_{DEX\ VS.\ DEX\ +\ TTX}$ = 0.0083 for **K**; one-way ANOVA with Tukey's multiple comparisons test). **L** Quantification of ELISA for total Tau levels in EV-depleted media from the indicated conditions, with values normalized to CON condition (***$P_{CON\ VS.\ DEX}$ = 0.0002, ***$P_{DEX\ VS.\ DEX\ +\ TTX}$ = 0.0002, one-way ANOVA with Tukey's multiple comparisons test). **M, N** Quantification of AT8/total Tau **M** and PHF1/total Tau **N** ratios, showing no significant difference between the indicated conditions ($P_{CON\ VS.\ DEX}$ = 0.9950, $P_{DEX\ VS.\ DEX\ +\ TTX}$ = 0.3951 for **M**, $P_{CON\ VS.\ DEX}$ = 0.6312, $P_{DEX\ VS.\ DEX\ +\ TDZD}$ = 0.2314 for **N**, one-way ANOVA with Tukey's multiple comparisons test). Data is presented as mean ± SEM with n = 3–4 samples/group (results were confirmed in two independent experiments).

are in line with other studies reporting that neuronal activity, in the form of depolarization or NMDA receptor activation, stimulates Tau phosphorylation [56, 57]. On the other hand, phosphorylated Tau can also exert effects on neuronal activity. In particular, the mislocalization of phospho-Tau species to dendritic spines in response to stress/GCs has been suggested to induce aberrant neuronal firing/excitotoxicity via Fyn kinase-mediated opening of NMDA receptors, leading to Ca^{2+} influx [14, 15, 57]. These findings suggest the existence of a positive feedback loop, wherein GC-induced neuronal activity promotes Tau phosphorylation, which in turn induces the synaptic mistargeting of phospho-Tau species that stimulate additional neuronal activity to continue this cycle. However, since GCs are known to activate multiple Tau kinases, including CDK5 and GSK3β [13, 40–42], and also to stimulate the firing of cortical and hippocampal glutamatergic neurons on a rapid timescale (1–4 h after application) [43–45], it may be challenging to fully disentangle the causality of these events.

Cumulatively, our data show that GC-mediated phosphorylation and oligomerization of Tau stimulates its vesicle-free secretion and trans-cellular spreading in a manner consistent with type 1 UPS. While questions remain about how Tau phosphorylation is precipitated by GCs, and how stress/GCs impact other forms of Tau propagation in the brain, this work provides some of the first mechanistic insight into how high GC levels accelerate pathogenic Tau spreading in AD and other tauopathies.

METHODS
Mice
Male and female C57BL/6 mice (obtained from the National Institute on Aging) and PS19 mice (obtained from The Jackson Laboratory; strain #008169) between the ages of 4–5 months were maintained under standard laboratory conditions with ad libitum access to food and water. All animal studies were carried out with the approval of the Columbia Institutional Animal Care and Use Committee (IACUC) in accordance with the National Institutes of Health guidelines for animal care, or the animal ethics committee of the University of Minho under protocol DGV9457, in accordance with the guidelines of the Portuguese national authority for animal experimentation, Direcção Geral de Veterinária, and Directive 2010/63/EU of the European Parliament and Council. Animal numbers (n) for experiments were obtained based on the estimated effect sizes calculated in our previous studies [15, 34]. This estimate uses a significance level of 0.05, mean group difference of 20–30%, standard error of the mean (SEM) values within the 10–20% range from the known mean of the population, and a power test of 0.80. Mice were allocated randomly into different groups as indicated.

Primary hippocampal culture
Primary mouse hippocampal neurons were prepared from postnatal day 0 wild-type or PS19 mice, as described previously [58], and maintained in 24-well plates with Neurobasal medium supplemented with B27, 600 μM L-glutamine, and antibiotic-antimycotic (all from ThermoFisher/Life Technologies). At 11–12 days in vitro (DIV), media was replaced with new media containing 0.5% B27 supplement and treated as follows: control (50% PEG400 diluted into media (vehicle for dex/mifepristone), dexamethasone (dex, 1 μM, #D2915, Sigma) for 48 h, mifepristone (5 μM, #S2606, Selleckchem) for 1-h pre-treatment + 48 h together with dex, NaClO$_3$ (50 mM, #403016, Sigma) for 24-h pre-treatment + 48 h together with dex, methyl-β-cyclodextrin (1 mM, #C4555, Sigma) for 24-h pre-treatment + 48 h with dex, TTX (1 μM, #554412, Sigma) for 24-h pre-treatment + 48 h together with dex, TDZD-8 (0.5 μM, #T8325, Sigma) for 24-h pre-treatment + 48 h together with dex. For all conditions, media was collected at 14 DIV. For LDH measurements (#C20300, ThermoFisher), media was collected from 14 DIV PS19 neurons with the indicated treatments.

Brain slice perfusion
Brains were harvested from mice sacrificed via cervical dislocation without anesthesia followed by decapitation [59]. Brain slices including cortex and hippocampus (coronal sections; 400 μm) were cut and maintained in an interface chamber at 29 °C and perfused with artificial cerebrospinal fluid (ACSF) continuously bubbled with 95% O$_2$ and 5% CO$_2$. ACSF composition was as follows: 124 mM NaCl, 4.4 mM KCl, 1 mM Na$_2$HPO$_4$, 25 mM NaHCO$_3$, 2 mM CaCl$_2$, 2 mM MgCl$_2$ and 10 mM glucose. ACSF was collected from ex vivo brain slices after the following treatments: control (50% PEG400 diluted into ACSF (dex/mifepristone vehicle), dexamethasone (5 μM) for 4 h, mifepristone (5 μM) for 1-h pre-treatment + 4 h with dex, NaClO$_3$ (100 mM), methyl-β-cyclodextrin (2.5 mM), or EGCG (50 μM, #E4113, Sigma) for 1.5-h pre-treatment + 4 h with dex.

### Media/ACSF preparation for immunoblot and ELISA
When indicated, the cell culture media or ACSF were centrifuged for 20 min at 2000 g to eliminate cell debris, then concentrated using Pierce™ Protein Concentrators PES with 30 K molecular-weight cutoff (Thermo-Fisher, #88531). To deplete extracellular vesicle (EVs), media/ACSF was subjected to sequential centrifugation steps: 30 min at 10,000 g, 30 min at 21,000 g, and finally 70 min at 100,000 g. The remaining supernatant was used for immunoblotting and ELISA.

CSF collection
Five-month-old C57BL/6 mice (13/group; 10 male and 3 female) were administered dexamethasone (D2915, Sigma; 5 mg/kg per day, dissolved in PBS, by intraperitoneal/i.p. injection), and mifepristone/RU486 (S2606, Selleckchem; 10 mg/kg per day, dissolved in 50% PEG400 in PBS, by i.p.) for 15 days. Control animals received injections of 50% PEG400 diluted in PBS. Following this treatment regimen, mice were euthanized by isoflurane and CSF was collected from the cisterna magna using a glass capillary.

Chronic unpredictable stress, brain tissue collection, and media harvest
Three- to four-month-old wild-type (C57BL/6 J) mice were housed in groups of 5–6 per cage under standard environmental conditions with ad libitum access to food and water. For the chronic unpredictable stress

Figure panels A–E
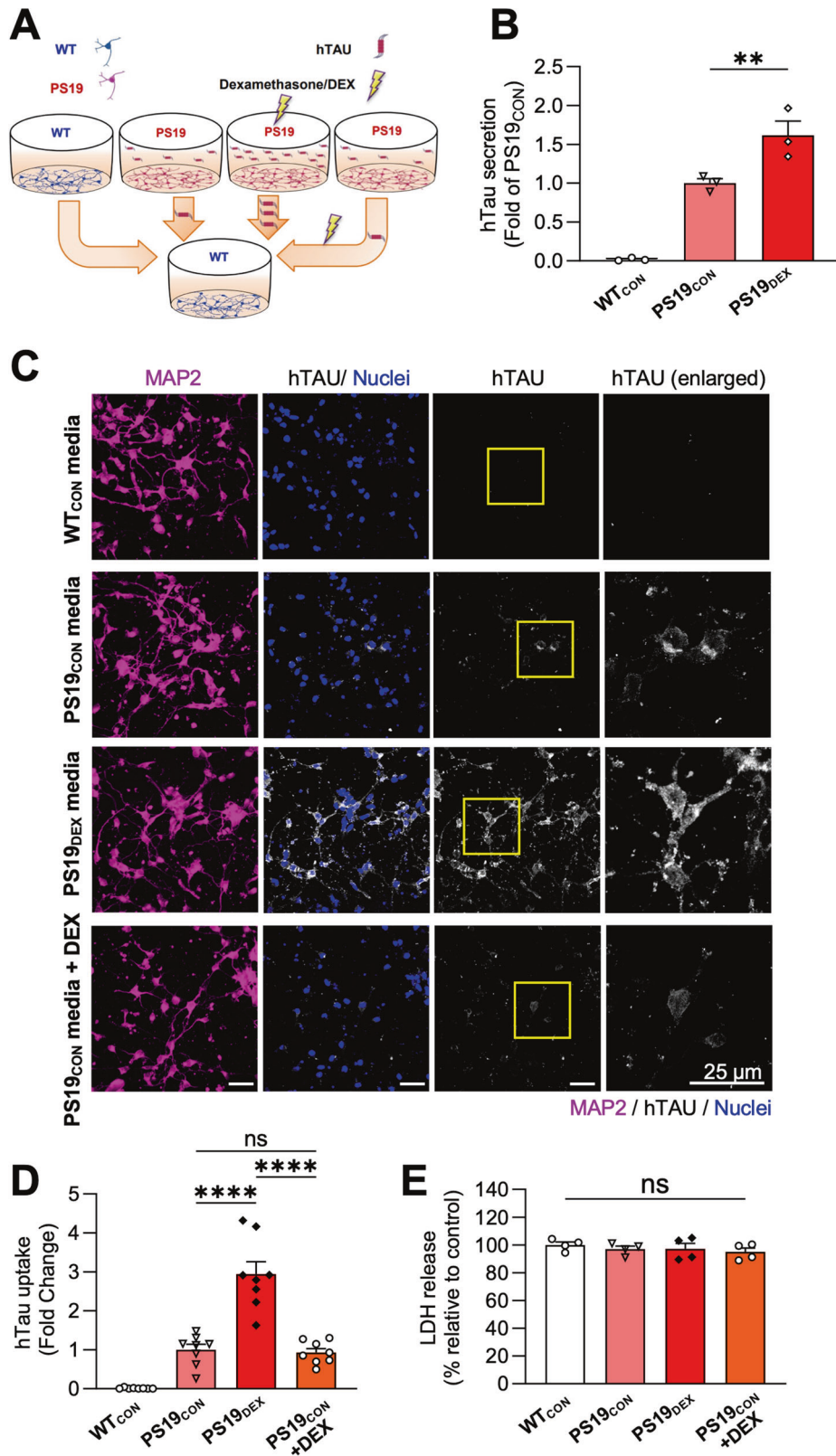
(CUS) protocol, animals were subjected to different stressors (i.e. 3 h overcrowding, 3 h rocking platform, 3 h restraint, 30 min hairdryer; one stressor per day) that were chosen randomly to prevent habituation, for 4–6 weeks, as previously described [15]. Stress efficacy was monitored by measurement of serum corticosterone levels at the nadir (a.m.) and zenith (p.m.) of secretion in the circadian cycle (measured by ELISA immunoassay,

ab108821, Abcam) and by body weight loss. Following the CUS protocol, animals were euthanized, brain tissue was immediately macrodissected and incubated in EV-release medium (Neurobasal medium, 1% Glutamax, 1% Anti-anti; ThermoFisher) for 16 h at 37 °C, 5% CO_2. Five hemi-cortices were pooled to obtain each cortical sample while hippocampi from 5 mouse brains were pooled into each hippocampal sample. After the

Fig. 4 GCs stimulate Tau secretion but not uptake by neurons. A Schematic diagram of experimental procedure for measuring Tau uptake in cultured neurons. **B** Quantification of ELISA for hTau levels in EV-depleted media from the indicated conditions, with values normalized to $PS19_{CON}$ condition (**$P_{PS19con\ VS.\ PS19dex}$ = 0.0019, *$P_{PS19dex\ VS.\ PS19con+DEX}$ = 0.0184; one-way ANOVA with Tukey's multiple comparisons test). **C** Representative images of wild-type recipient hippocampal neurons immunostained for MAP2 (pink) and human-specific Tau (hTau, white), following 48-hour incubation with media from: WT donor neurons treated with vehicle control for 48 h (WT_{CON}), PS19 donor neurons treated with vehicle for 48 h ($PS19_{CON}$), PS19 donor neurons treated with DEX for 48 h ($PS19_{DEX}$), or PS19 donor neurons treated with vehicle for 48 h, with DEX added to recipient neurons ($PS19_{CON}$ + DEX). Nuclei are stained with DAPI. Scale bar, 25 μm. **D** Quantification of Tau uptake by recipient neurons, measured by hTau fluorescence intensity and normalized to $PS19_{CON}$ condition (****$P_{PS19CON\ VS.\ PS19DEX}$ < 0.0001, ****$P_{PS19DEX\ VS.\ PS19con+DEX}$ < 0.0001; one-way ANOVA with Tukey's multiple comparisons test; n = 8 fields of view/condition). **E** Quantification of LDH release showing no difference between the conditions (ns, one-way ANOVA with Tukey's multiple comparisons test). Data is presented as mean ± SEM with n = 3–4 samples/group (results were confirmed in two independent experiments).

incubation period, media was collected and subject to extracellular vesicle depletion as described above (Media/ACSF preparation).

ExoView imager analysis

The characterization and quantification of exosomes in hippocampal culture media were performed according to the manufacturer's instructions [60]. Briefly, chips containing capture probes coated with antibodies against two exosome-enriched tetraspanins, CD81 and CD9, were pre-scanned to acquire baseline particle adhesion prior to sample incubation. Media samples were diluted to fall within the dynamic range of the Exoview R100 instrument (Unchained Labs) and incubated overnight at room temperature on the pre-scanned chips in a sealed 24-well plate. The chips were then washed to remove any non-captured material, incubated for 1 h at room temperature with fluorescently-conjugated antibodies against CD9, CD63, and CD81, washed again, dried, and then scanned with the ExoView R100 system to obtain data on particle counts, size, and exosome surface membrane protein profiles. For each capture probe (CD9 and CD81), background particle readout is subtracted from the final particle count to produce a final exosome count readout.

Immunoblotting

The concentrated media/ACSF with extracellular vesicle (EV) depletion were prepared in 4x Laemmli buffer and then boiled for 5 min. Samples were either dotted directly onto nitrocellulose membranes for dot blotting or separated by SDS/PAGE (10% Tris-Glycine gel; XP00105BOX, Invitrogen) and then transferred to a nitrocellulose membrane (10600001, Amersham). After blocking in TBST buffer (20 mM Tris-HCl, 150 mM sodium chloride, 0.1% Tween-20) containing 5% (wt/vol) nonfat dry milk for 1 h at room temperature, the membrane was incubated with primary antibodies overnight at 4 °C, then with secondary antibodies for 1 h at room temperature. The following antibodies were used: Tau5 (ab80579, Abcam), AT8: anti-phospho-Tau pSer202/Thr205 (MN1020, ThermoFisher), PHF-1: anti-phospho-Tau pSer396/Ser404 Tau (from Dr. Peter Davies), p-GR (4161 S, Cell Signaling), GR (12041 S, Cell Signaling), β-actin (4967 S, cell signaling), anti-Tubulin (ab4074, Abcam). IRDye 800CW goat anti-mouse IgG secondary antibody (P/N: 926-32210, LI-COR), IRDye 680CW goat anti-rabbit IgG secondary antibody (P/N: 926-68071, LI-COR). Membranes were visualized by Odyssey Infrared Imager (model 9120, LI-COR Biosciences), and relative optical densities of bands determined by Fiji/ImageJ software. Full immunoblots used in the figures of this manuscript are shown in Fig. S4.

ELISA

EV-depleted media/ACSF samples (50 μL volume) were used for measurement of Tau concentration by a mouse-specific total Tau ELISA kit (KMB7011, ThermoFisher), pS199 Tau ELISA kit (KMB7041) or human total Tau ELISA kit (KHB0041, ThermoFisher) according to manufacturer's instructions.

Tau uptake assay

Media was collected from donor WT or PS19 neurons treated with vehicle control or dex (1 μM) for 48 h. The media from these cultures was then depleted of EVs as described above and transferred to naïve recipient wild-type neurons for a 48-h incubation. For one condition, recipient neurons were also treated with dex (1 μM) during this time. Following incubation, recipient cells were washed three times with cold 1× PBS and fixed with 4% paraformaldehyde, as previously described [58]. The uptake of hTau was then detected by immunostaining with MAP2 and Tau13 antibodies as described below.

Immunofluorescence staining of brain slices, cultured neurons

Floating brain sections or fixed primary neurons were immunostained as previously described [58]. Briefly, fixed neurons or slices cut at 35 μm on a vibratome (VT1000S; Leica) were incubated overnight with the following primary antibodies: mouse Anti-Tau, 15–25 (Tau-13) antibody (1:1000, 835201, BioLegend) and chicken MAP2 (1:5000, ab5392, Abcam). They were then incubated for 1 h with secondary antibodies (Alexa Fluor® 594 anti-mouse IgG, and Alexa Fluor® 633 anti-chicken IgG, 1:2000 dilution). Coverslips were mounted with VectaShield (Vector Laboratories) and sealed with clear nail polish. Images were acquired with either a 63× objective (Neofluar, NA 1.4) or a 10X objective (for lower magnification images in Figure S3A-D) on a Zeiss LSM 800 confocal microscope running Zen2 software. The images were manually measured and quantified using the auto-threshold settings in Fiji/ImageJ software.

AAV injection procedure

The AAV.CBA.eGFP.2 A.P301L-Tau plasmid, a gift from Bradley Hyman (Addgene plasmid #140425; http://n2t.net/addgene:140425;RRID :Addgene_140425), was packaged into AAV8 serotype by University of Pennsylvania Viral Vector Core. Prior to AAV injection, male/female mice (3–4/group) were administered dex (5 mg/kg, i.p.injection)±mifepristone (10 mg/kg, i.p. injection) or dex (5 mg/kg, i.p. injection)±EGCG (20 mg/kg, i.p. injection) for 7 days. Stereotactic AAV injections were performed under standard aseptic surgery conditions as previously described [47]. Briefly, mice were anaesthetized with isoflurane (2%), placed in a stereotactic frame (digital stereotaxic device, Stoelting Co.), and injected bilaterally with 2 μl of AAV in hippocampal region CA1 (at the following coordinates relative to Bregma: A/P − 2.7 mm, M/L ± 2 mm, D/V − 1.5 mm) with a 10 μl Hamilton syringe at a rate of 0.25 μl/min by a Nano-injector system (Stoelting microsyringe pump, Stoelting Co.). The needle was kept in place for an additional 5 min. Afterwards, the skin over the injection site was sutured and mice were placed on a warming pad during their recovery from anesthesia. Mice were then administered dex with or without mifepristone or EGCG for an additional 14 days prior to euthanasia and brain harvest. Control animals received daily i.p. injections of 50% PEG400 in PBS (dex/mifepristone vehicle) or PBS (dex/EGCG vehicle).

Quantification of Tau spreading

hTau$^+$ neurons (detected by immunostaining with Tau13 antibody) were counted in the hippocampi of coronal brain sections near the site of AAV injection (A/P −2.7 mm, M/L ± 2 mm, D/V − 1.5 mm relative to Bregma; identified by the dense cluster of GFP$^+$ neurons). Tau spreading was quantified as in previous studies [46, 47], by calculating the number of hTau$^+$ neurons in the hippocampus that did not exhibit GFP fluorescence (hTau$^+$/GFP$^-$ neurons) per mm^2 and the fraction of hTau$^+$ cells that were GFP$^+$ (GFP/hTau colocalization). For each condition, we also measured the maximum distance between hTau$^+$ neurons in the vicinity of the hippocampal formation and the cluster of GFP$^+$ neurons near the injection site (see Fig. S3A–D), using the Fiji/Image J measurement tools.

Statistical analysis

All values were expressed as the mean ± SEM. All graphing and statistical analyses were performed using GraphPad Prism (GraphPad Prism9.Ink). Statistical details of experiments are provided in the figure legends. Statistical analyses were performed with unpaired, two-tailed t-test or one-way ANOVA with Tukey's test for multiple comparisons. Values of $p < 0.05$ were considered statistically significant. *$p < 0.05$,
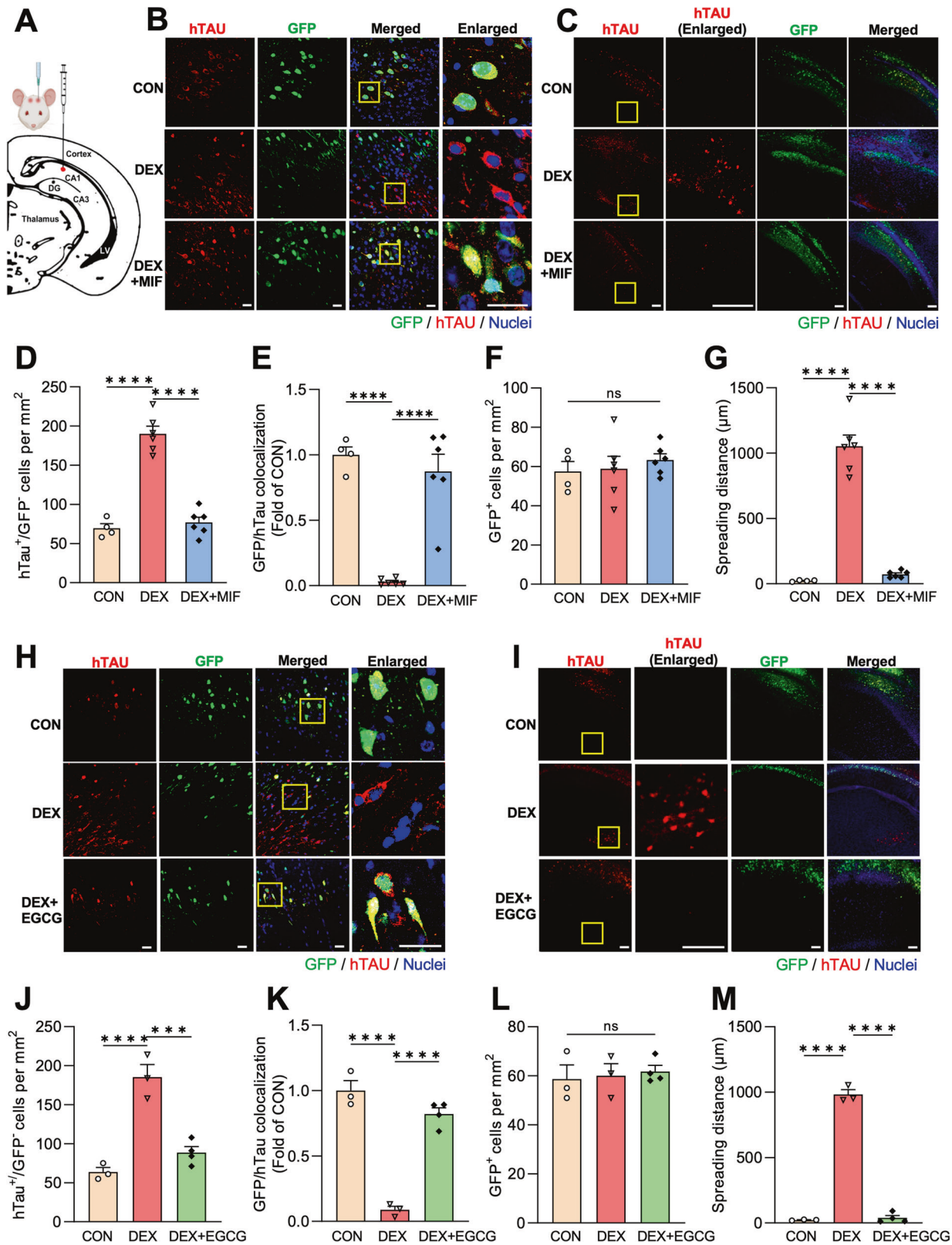
Fig. 5 GCs induce Tau spreading in vivo that is attenuated by EGCG. A Schematic diagram indicating the AAV injection site in murine hippocampal area CA1. **B** Representative images showing hTau (red) and GFP (green) in CA1 neurons of mice treated with vehicle (CON), dexamethasone (DEX), or DEX + MIF. Nuclei are stained with DAPI (blue). Right column shows enlarged regions (indicated by yellow boxes). Scale bars, 50 μm. **C** Representative images depicting the spreading of hTau (red) from GFP$^+$ cells near the injection site in mice treated as indicated. Note hTau spreading beyond area CA1 in the DEX condition only (yellow box). Scale bars, 200 μm. **D** Quantification of hTau$^+$/GFP$^-$ cells per mm^2 in mice treated as indicated ($****P_{CON \text{ vs. } DEX} < 0.0001$, $****P_{DEX \text{ vs. } DEX + MIF} < 0.0001$, one-way ANOVA with Tukey's multiple comparisons test). **E** Quantification of the GFP/hTau colocalization ratio in each condition, normalized to CON condition ($****P_{CON \text{ vs. } DEX} < 0.0001$, $****P_{DEX \text{ vs. } DEX + MIF} < 0.0001$, one-way ANOVA with Tukey's multiple comparisons test). **F** Quantification of GFP$^+$ cells per mm^2 in mice treated as indicated ($P_{CON \text{ vs. } DEX} = 0.9833$, $P_{DEX \text{ vs. } DEX + MIF} = 0.7897$, one-way ANOVA with Tukey's multiple comparisons test). **G** Quantification of Tau spreading distance for each condition ($****P_{CON \text{ vs. } DEX} < 0.0001$, $****P_{DEX \text{ vs. } DEX + MIF} < 0.0001$, one-way ANOVA with Tukey's multiple comparisons test). **H–I** Representative images showing hTau/GFP colocalization **H** and spreading **I** for mice treated as indicated. **J** Quantification of hTau$^+$/GFP$^-$ cells per mm^2 in mice treated as indicated ($***P_{CON \text{ vs. } DEX} = 0.0003$, $***P_{DEX \text{ vs. } DEX + EGCG} = 0.0007$, one-way ANOVA with Tukey's multiple comparisons test). **K** Quantification of the GFP/hTau colocalization ratio in each condition, normalized to CON condition ($****P_{CON \text{ vs. } DEX} < 0.0001$, $****P_{DEX \text{ vs. } DEX + EGCG} < 0.0001$, one-way ANOVA with Tukey's multiple comparisons test). **L** Quantification of GFP$^+$ cells per mm^2 in mice treated as indicated ($P_{CON \text{ vs. } DEX} = 0.9760$, $P_{DEX \text{ vs. } DEX + EGCG} = 0.9534$, one-way ANOVA with Tukey's multiple comparisons test). **M** Quantification of Tau spreading distance for each condition ($****P_{CON \text{ vs. } DEX} < 0.0001$, $****P_{DEX \text{ vs. } DEX + EGCG} < 0.0001$, one-way ANOVA with Tukey's multiple comparisons test). Data is presented as mean ± SEM with $n = 4$–6 mice/group. Each point represents an individual mouse.

◄

$**p < 0.01$, $***p < 0.001$, $****p < 0.0001$. Investigators were blinded to treatment conditions when performing analyses for all experiments.

DATA AVAILABILITY
The experimental data sets generated and/or analyzed during this study are available from the corresponding author upon reasonable request.

REFERENCES
1. Caruso A, Nicoletti F, Gaetano A, Scaccianoce S. Risk factors for Alzheimer's disease: focus on stress. Front Pharmacol. 2019;10:976.
2. Mravec B, Horvathova L, Padova A. Brain under stress and Alzheimer's disease. Cell Mol Neurobiol. 2018;38:73–84.
3. Machado A, Herrera AJ, de Pablos RM, Espinosa-Oliva AM, Sarmiento M, Ayala A, et al. Chronic stress as a risk factor for Alzheimer's disease. Rev Neurosci. 2014;25:785–804.
4. Johansson L, Guo X, Waern M, Ostling S, Gustafson D, Bengtsson C, et al. Midlife psychological stress and risk of dementia: a 35-year longitudinal population study. Brain. 2010;133:2217–24.
5. Huang CW, Lui CC, Chang WN, Lu CH, Wang YL, Chang CC. Elevated basal cortisol level predicts lower hippocampal volume and cognitive decline in Alzheimer's disease. J Clin Neurosci. 2009;16:1283–6.
6. Mejia S, Giraldo M, Pineda D, Ardila A, Lopera F. Nongenetic factors as modifiers of the age of onset of familial Alzheimer's disease. Int Psychogeriatrics. 2003;15:337–49.
7. Green KN, Billings LM, Roozendaal B, McGaugh JL, LaFerla FM. Glucocorticoids increase amyloid-beta and tau pathology in a mouse model of Alzheimer's disease. J Neurosci. 2006;26:9047–56.
8. Han B, Yu L, Geng Y, Shen L, Wang H, Wang Y, et al. Chronic Stress Aggravates Cognitive Impairment and Suppresses Insulin Associated Signaling Pathway in APP/PS1 Mice. J Alzheimers Dis. 2016;53:1539–52.
9. Jeong YH, Park CH, Yoo J, Shin KY, Ahn SM, Kim HS, et al. Chronic stress accelerates learning and memory impairments and increases amyloid deposition in APPV717I-CT100 transgenic mice, an Alzheimer's disease model. FASEB J. 2006;20:729–31.
10. Carroll JC, Iba M, Bangasser DA, Valentino RJ, James MJ, Brunden KR, et al. Chronic stress exacerbates tau pathology, neurodegeneration, and cognitive performance through a corticotropin-releasing factor receptor-dependent mechanism in a transgenic mouse model of tauopathy. J Neurosci. 2011;31:14436–49.
11. Baglietto-Vargas D, Chen Y, Suh D, Ager RR, Rodriguez-Ortiz CJ, Medeiros R, et al. Short-term modern life-like stress exacerbates Abeta-pathology and synapse loss in 3xTg-AD mice. J Neurochem. 2015;134:915–26.
12. Dong H, Goico B, Martin M, Csernansky CA, Bertchume A, Csernansky JG. Modulation of hippocampal cell proliferation, memory, and amyloid plaque deposition in APPsw (Tg2576) mutant mice by isolation stress. Neuroscience. 2004;127:601–9.
13. Sotiropoulos I, Catania C, Pinto LG, Silva R, Pollerberg GE, Takashima A, et al. Stress acts cumulatively to precipitate Alzheimer's disease-like tau pathology and cognitive deficits. J Neurosci. 2011;31:7840–7.
14. Pinheiro S, Silva J, Mota C, Vaz-Silva J, Veloso A, Pinto V, et al. Tau mislocation in glucocorticoid-triggered hippocampal pathology. Mol Neurobiol. 2016;53:4745–53.
15. Lopes S, Vaz-Silva J, Pinto V, Dalla C, Kokras N, Bedenk B, et al. Tau protein is essential for stress-induced brain pathology. Proc Natl Acad Sci USA. 2016;113:E3755–63.
16. Roberson ED, Scearce-Levie K, Palop JJ, Yan F, Cheng IH, Wu T, et al. Reducing endogenous tau ameliorates amyloid beta-induced deficits in an Alzheimer's disease mouse model. Science. 2007;316:750–4.
17. Vossel KA, Zhang K, Brodbeck J, Daub AC, Sharma P, Finkbeiner S, et al. Tau reduction prevents Abeta-induced defects in axonal transport. Science. 2010;330:198.
18. Braak H, Braak E. Neuropathological stageing of Alzheimer-related changes. Acta Neuropathol. 1991;82:239–59.
19. Bejanin A, Schonhaut DR, La Joie R, Kramer JH, Baker SL, Sosa N, et al. Tau pathology and neurodegeneration contribute to cognitive impairment in Alzheimer's disease. Brain. 2017;140:3286–300.
20. Nelson PT, Alafuzoff I, Bigio EH, Bouras C, Braak H, Cairns NJ, et al. Correlation of Alzheimer disease neuropathologic changes with cognitive status: a review of the literature. J Neuropathol Exp Neurol. 2012;71:362–81.
21. DeLeo AM, Ikezu T. Extracellular vesicle biology in Alzheimer's disease and related tauopathy. J Neuroimmune Pharmacol. 2018;13:292–308.
22. Brunello CA, Merezhko M, Uronen RL, Huttunen HJ. Mechanisms of secretion and spreading of pathological tau protein. Cell Mol Life Sci. 2020;77:1721–44.
23. Dujardin S, Begard S, Caillierez R, Lachaud C, Delattre L, Carrier S, et al. Ectosomes: a new mechanism for non-exosomal secretion of tau protein. PLoS ONE. 2014;9:e100760.
24. Asai H, Ikezu S, Tsunoda S, Medalla M, Luebke J, Haydar T, et al. Depletion of microglia and inhibition of exosome synthesis halt tau propagation. Nat Neurosci. 2015;18:1584–93.
25. Wang Y, Balaji V, Kaniyappan S, Kruger L, Irsen S, Tepper K, et al. The release and trans-synaptic transmission of Tau via exosomes. Mol Neurodegen. 2017;12:5.
26. Pooler AM, Phillips EC, Lau DH, Noble W, Hanger DP. Physiological release of endogenous tau is stimulated by neuronal activity. EMBO Rep. 2013;14:389–94.
27. Chai X, Dage JL, Citron M. Constitutive secretion of tau protein by an unconventional mechanism. Neurobiol Dis. 2012;48:356–66.
28. Fontaine SN, Zheng D, Sabbagh JJ, Martin MD, Chaput D, Darling A, et al. DnaJ/Hsc70 chaperone complexes control the extracellular release of neurodegenerative-associated proteins. EMBO J. 2016;35:1537–49.
29. Wu JW, Hussaini SA, Bastille IM, Rodriguez GA, Mrejeru A, Rilett K, et al. Neuronal activity enhances tau propagation and tau pathology in vivo. Nat Neurosci. 2016;19:1085–92.
30. Guix FX, Corbett GT, Cha DJ, Mustapic M, Liu W, Mengel D, et al. Detection of aggregation-competent Tau in neuron-derived extracellular vesicles. Int J Mol Sci. 2018;19:663.
31. Wegmann S, Nicholls S, Takeda S, Fan Z, Hyman BT. Formation, release, and internalization of stable tau oligomers in cells. J Neurochem. 2016;139:1163–74.
32. Faure J, Lachenal G, Court M, Hirrlinger J, Chatellard-Causse C, Blot B, et al. Exosomes are released by cultured cortical neurones. Mol Cell Neurosci. 2006;31:642–8.
33. Lopes S, Teplytska L, Vaz-Silva J, Dioli C, Trindade R, Morais M, et al. Tau deletion prevents stress-induced dendritic atrophy in prefrontal cortex: role of synaptic mitochondria. Cereb Cortex. 2017;27:2580–91.
34. Du F, Yu Q, Swerdlow RH, Waites CL. Glucocorticoid-driven mitochondrial damage stimulates Tau pathology. Brain. 2023;146:4378–94.

35. Lasagna-Reeves CA, Castillo-Carranza DL, Sengupta U, Sarmiento J, Troncoso J, Jackson GR, et al. Identification of oligomers at early stages of tau aggregation in Alzheimer's disease. FASEB J. 2012;26:1946–59.

36. Thery C, Amigorena S, Raposo G, Clayton A. Isolation and characterization of exosomes from cell culture supernatants and biological fluids. Current protocols in cell biology/editorial board, Juan S Bonifacino [et al]. 2006;Chapter 3:Unit 3 22.

37. Keerthikumar S, Gangoda L, Liem M, Fonseka P, Atukorala I, Ozcitti C, et al. Proteogenomic analysis reveals exosomes are more oncogenic than ectosomes. Oncotarget. 2015;6:15375–96.

38. Merezhko M, Brunello CA, Yan X, Vihinen H, Jokitalo E, Uronen RL, et al. Secretion of Tau via an unconventional non-vesicular mechanism. Cell Rep. 2018;25:2027–2035.e4.

39. Katsinelos T, Zeitler M, Dimou E, Karakatsani A, Muller HM, Nachman E, et al. Unconventional Secretion Mediates the Trans-cellular Spreading of Tau. Cell reports. 2018;23:2039–55.

40. Sotiropoulos I, Catania C, Riedemann T, Fry JP, Breen KC, Michaelidis TM, et al. Glucocorticoids trigger Alzheimer disease-like pathobiochemistry in rat neuronal cells expressing human tau. J Neurochem. 2008;107:385–97.

41. Yi JH, Brown C, Whitehead G, Piers T, Lee YS, Perez CM, et al. Glucocorticoids activate a synapse weakening pathway culminating in tau phosphorylation in the hippocampus. Pharmacol Res. 2017;121:42–51.

42. Dey A, Hao S, Wosiski-Kuhn M, Stranahan AM. Glucocorticoid-mediated activation of GSK3beta promotes tau phosphorylation and impairs memory in type 2 diabetes. Neurobiol Aging. 2017;57:75–83.

43. Beck SG, List TJ, Choi KC. Long- and short-term administration of corticosterone alters CA1 hippocampal neuronal properties. Neuroendocrinology. 1994;60:261–72.

44. Joels M. Stress, the hippocampus, and epilepsy. Epilepsia. 2009;50:586–97.

45. Krugers HJ, Alfarez DN, Karst H, Parashkouhi K, van Gemert N, Joels M. Corticosterone shifts different forms of synaptic potentiation in opposite directions. Hippocampus. 2005;15:697–703.

46. Wegmann S, Bennett RE, Delorme L, Robbins AB, Hu M, McKenzie D, et al. Experimental evidence for the age dependence of tau protein spread in the brain. Sci Adv. 2019;5:eaaw6404.

47. Rauch JN, Luna G, Guzman E, Audouard M, Challis C, Sibih YE, et al. LRP1 is a master regulator of tau uptake and spread. Nature. 2020;580:381–5.

48. Wobst HJ, Sharma A, Diamond MI, Wanker EE, Bieschke J. The green tea polyphenol (-)-epigallocatechin gallate prevents the aggregation of tau protein into toxic oligomers at substoichiometric ratios. FEBS Lett. 2015;589:77–83.

49. Gosselet F, Loiola RA, Roig A, Rosell A, Culot M. Central nervous system delivery of molecules across the blood-brain barrier. Neurochem Int. 2021;144:104952.

50. Ali SN, Arif A, Ansari FA, Mahmood R. Cytoprotective effect of taurine against sodium chlorate-induced oxidative damage in human red blood cells: an ex vivo study. Amino Acids. 2022;54:33–46.

51. Merezhko M, Uronen RL, Huttunen HJ. The cell biology of Tau secretion. Front Mol Neurosci. 2020;13:569818.

52. Patra SK, Rizzi F, Silva A, Rugina DO, Bettuzzi S. Molecular targets of (-)-epigallocatechin-3-gallate (EGCG): specificity and interaction with membrane lipid rafts. J Physiol Pharmacol. 2008;59:217–35.

53. Sun Y, Hung WC, Chen FY, Lee CC, Huang HW. Interaction of tea catechin (-)-epigallocatechin gallate with lipid bilayers. Biophys J. 2009;96:1026–35.

54. Balasubramaniam M, Mainali N, Bowroju SK, Atluri P, Penthala NR, Ayyadevera S, et al. Structural modeling of GSK3beta implicates the inactive (DFG-out) conformation as the target bound by TDZD analogs. Sci Rep. 2020;10:18326.

55. Sayas CL, Avila J. GSK-3 and Tau: A Key Duet in Alzheimer's Disease. Cells. 2021;10:721.

56. Pierrot N, Santos SF, Feyt C, Morel M, Brion JP, Octave JN. Calcium-mediated transient phosphorylation of tau and amyloid precursor protein followed by intraneuronal amyloid-beta accumulation. J Biol Chem. 2006;281:39907–14.

57. Hu Z, Ondrejcak T, Yu P, Zhang Y, Yang Y, Klyubin I, et al. Do tau-synaptic long-term depression interactions in the hippocampus play a pivotal role in the progression of Alzheimer's disease? Neural Regen Res. 2023;18:1213–9.

58. Du F, Yu Q, Yan S, Hu G, Lue LF, Walker DG, et al. PINK1 signalling rescues amyloid pathology and mitochondrial dysfunction in Alzheimer's disease. Brain. 2017;140:3233–51.

59. Yu Q, Wang Y, Du F, Yan S, Hu G, Origlia N, et al. Overexpression of endophilin A1 exacerbates synaptic alterations in a mouse model of Alzheimer's disease. Nat Commun. 2018;9:2968.

60. Breitwieser K, Koch LF, Tertel T, Proestler E, Burgers LD, Lipps C, et al. Detailed characterization of small extracellular vesicles from different cell types based on tetraspanin composition by ExoView R100 platform. Int J Mol Sci. 2022;23:8544.

ACKNOWLEDGEMENTS

AUTHOR CONTRIBUTIONS
QY, FD, IS, and CLW designed the research; QY, FD, IB and PG performed experiments and analyzed data; IS and CLW supervised experiments; CLW wrote the manuscript; QY and FD prepared figures; QY, FD, PG, IS and CLW edited the manuscript. All authors read and approved the final manuscript.

COMPETING INTERESTS
The authors declare no competing interests.

ETHICS
All animal studies were carried out with the approval of either the Columbia Institutional Animal Care and Use Committee (IACUC) under protocol AABK15555, in accordance with the National Institutes of Health guidelines for animal care, or the animal ethics committee of the University of Minho under protocol DGV9457, in accordance with the guidelines of the Portuguese national authority for animal experimentation, Direcção Geral de Veterinária, and Directive 2010/63/EU of the European Parliament and Council.

ADDITIONAL INFORMATION
Supplementary information The online version contains supplementary material available at https://doi.org/10.1038/s41419-024-06458-3.

Correspondence and requests for materials should be addressed to Clarissa L. Waites.

Reprints and permission information is available at http://www.nature.com/reprints

Publisher's note Springer Nature remains neutral with regard to jurisdictional claims in published maps and institutional affiliations.